Journal of Medicinal Chemistry

Article

Theoretical and Experimental Design of Atypical Kinase Inhibitors: Application to p38 MAP Kinase

Kim F. McClure, Yuriy A. Abramov, Ellen R. Laird, John T. Barberia, Weiling Cai, Thomas J. Carty, Santo R. Cortina, Dennis E. Danley, Alan J. Dipesa, Kathleen M. Donahue, Mark A. Dombroski, Nancy C. Elliott, Christopher A. Gabel, Seungil Han, Thomas R. Hynes, Peter K. LeMotte, Mahmoud N. Mansour, Eric S. Marr, Michael A. Letavic, Jayvardhan Pandit, David B. Ripin, Francis J. Sweeney, Douglas Tan, and Yong Tao

J. Med. Chem., **2005**, 48 (18), 5728-5737• DOI: 10.1021/jm050346q • Publication Date (Web): 05 August 2005

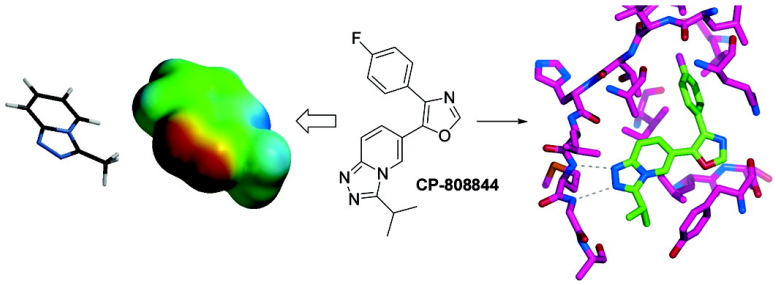

More About This Article

Additional resources and features associated with this article are available within the HTML version:

- Supporting Information
- Links to the 4 articles that cite this article, as of the time of this article download
- Access to high resolution figures
- Links to articles and content related to this article
- Copyright permission to reproduce figures and/or text from this article

View the Full Text HTML

Journal of Medicinal Chemistry is published by the American Chemical Society. 1155 Sixteenth Street N.W., Washington, DC 20036

Theoretical and Experimental Design of Atypical Kinase Inhibitors: Application to p38 MAP Kinase

Kim F. McClure,* Yuriy A. Abramov,* Ellen R. Laird, John T. Barberia, Weiling Cai, Thomas J. Carty, Santo R. Cortina, Dennis E. Danley, Alan J. Dipesa, Kathleen M. Donahue, Mark A. Dombroski, Nancy C. Elliott, Christopher A. Gabel, Seungil Han, Thomas R. Hynes, Peter K. LeMotte, Mahmoud N. Mansour, Eric S. Marr, Michael A. Letavic, Jayvardhan Pandit, David B. Ripin, Francis J. Sweeney, Douglas Tan, and Yong Tao

Pfizer Global Research and Development, Groton Laboratories, Eastern Point Road, Groton, Connecticut 06340

Received April 13, 2005

Mimics of the benzimidazolone nucleus found in inhibitors of p38 kinase are proposed, and their theoretical potential as bioisosteres is described. A set of calculated descriptors relevant to the anticipated binding interaction for the fragments 1-methyl-1*H*-benzotriazole **5**, 3-methylbenzo[*d*]isoxazole **3**, and 3-methyl-[1,2,4]triazolo[4,3-*a*]pyridine **4**, pyridine **1**, and 1,3-dimethyl-1,3-dihydro-benzoimidazol-2-one **2** are reported. The design considerations and synthesis of p38 inhibitors based on these H-bond acceptor fragments is detailed. Comparative evaluation of the pyridine-, benzimidazolone-, benzotriazole-, and triazolopyridine-based inhibitors shows the triazoles **20** and **25** to be significantly more potent experimentally than the benzimidazolone after which they were modeled. An X-ray crystal structure of **25** bound to the active site shows that the triazole group serves as the H-bond acceptor but unexpectedly as a dual acceptor, inducing movement of the crossover connection of p38α. The computed descriptors for the hydrophobic and $\pi-\pi$ interaction capacities were the most useful in ranking potency.

Introduction

In the development of potential drug candidates, lead compounds are subject to a variety of modifications with the goal of improving the druglike qualities of the molecule. In many instances, the changes include substitution of one group for another or bioisosteric changes.[1−3] When one designs bioisosteres it is important to consider the steric and electronic properties of the group being replaced. Knowledge of the presence or absence of hydrogen bonding (H-bonding) interactions is also important in contemplating molecular replacements. Intermolecular hydrogen bonding plays a crucial role in a ligand−protein binding; it outlines the specificity of the interaction and counterbalances desolvation penalties of both the ligand and the binding site. Herein we describe a computational evaluation of several heterocyclic systems intended to replace a typically conserved H-bonding pattern of a ligand−kinase binding interaction. While our work is specific to the p38α kinase enzyme, the approach is applicable to other protein−ligand interactions in general.

The stress-activated protein kinase p38α is part of a complex cytokine-signaling pathway. Small-molecule inhibitors of p38α have demonstrated antiinflammatory properties in vivo[4−6] and have great potential in the treatment of conditions such as rheumatoid arthritis, psoriasis, COPD, and inflammatory bowel disease. The X-ray crystal structure of the enzyme has been solved with various inhibitors bound in the ATP binding pocket.[7−10] One of the key interactions in these structures is a hydrogen bond between the inhibitor and the flexible strand referred to as the crossover connection.[11] This connection is also described as the hinge region and connects the N-terminal and C-terminal lobes of the kinase.

Previously, we described a series of benzimidazolone p38 inhibitors,[12] wherein we proposed that the imidazolone carbonyl participated in this important H-bond with Met109NH of the crossover connection. The remainder of the molecule is believed to occupy the ATP binding site of p38α in a manner analogous to the prototypical pyridyl-imidazole inhibitors[9] (see Figure 1; left). To model such benzimidazolone inhibitors into the published active site seen with pyridyl-imidazole inhibitors, small movements of the protein were required to accommodate the span of the benzimidazolone group between the core imidazole ring and the H-bond donor Met109NH (see Figure 1; right). Although we could not structurally confirm this mode of binding, it is supported by the structure−activity relationship (SAR), which, despite the greater spatial requirements of the benzimidazolone, parallels that of the pyridyl-imidazoles.[12] Since the only published H-bond acceptor alternatives to pyridine, at that time, were very close-in permutations such as pyrimidines, the benzimidazolone nucleus represented a unique example of a significantly larger group serving in the same role.

As part of our effort to improve our benzimidazolone p38 inhibitors we set out to find outright replacements for the benzimidazolone group. Herein we report a computational evaluation of these alternatives and the experimental follow-up of selected analogues compared with their pyridine and benzimidazolone counterparts.

One of the concerns with the hypothetical binding mode for the benzimidazolones (shown in Figure 1) had

* To whom correspondence should be addressed. K.F.M.−Phone: (860) 441-8223. Fax: (860) 715-4610. E-mail: kim.f.mcclure@pfizer.com. Y.A.A.−Phone (860) 715-6005. Fax: (860) 441-4734. E-mail: yuriy.a.abramov@pfizer.com.

10.1021/jm050346q CCC: $30.25
Published on Web 08/05/2005

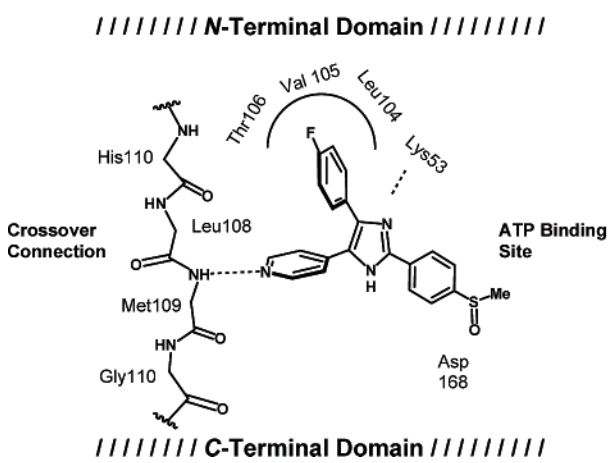

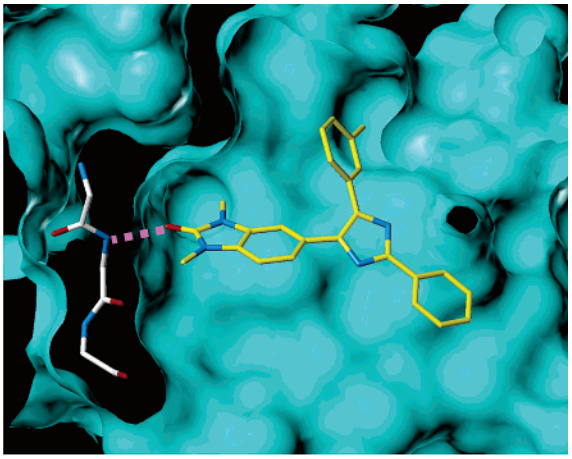

Figure 1. Cartoon representation (left) of p38α−SB-203580 complex 1IAN and model (right) of a benzimidazolone in the active site of p38α. See Supporting Information for details on the model.

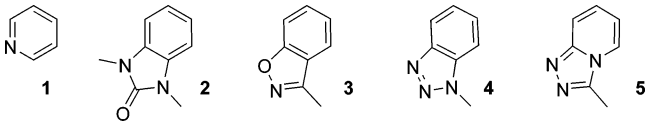

Figure 2. Structure of H-bond acceptor fragments.

to do with the added size of the benzimidazolone H-bond acceptor group relative to pyridine. In thinking of alternative H-bond acceptors that could be used, an emphasis was placed on molecules that were intermediate in size relative to pyridine and benzimidazolone.[13] Another concern was with the dual acceptor potential of the imidazolone carbonyl oxygen and whether this potential is realized in the H-bond contact with the crossover connection Met109NH and neighboring residues. The available structural information in the literature at the time only exemplified single H-bond acceptor or acceptor donor patterns. A loss in potency should accompany compounds with unsatisfied H-bond acceptor sites.

With this in mind, our thinking centered on benzofused hetereocyclic systems smaller than benzimidazolone that would still project two potential H-bond acceptors.[14] Three ideas fitting our criteria, along with pyridine **1** and dimethylbenzimidazolone **2**, are shown in Figure 2. Because single heteroatom benzofused systems would either have hydrogens (e.g., 2*H*-isoindole) or have orthogonally disposed lone pairs (e.g., isobenzofuran, benzo[*c*]thiophene) relative to the benzimidazolone carbonyl oxygen, all our proposed replacements separated the H-bond acceptors onto two adjacent atoms. While other possibilities could also have been explored, the unusual dual acceptor feature being proposed warranted a cautious approach given the lack of precedent.

Computational Approach

The templates **3**−**5** were theoretically compared with the known reference templates pyridine and the benzimidazolone **2**. The best template should display optimal nonbonding interactions with the kinase, which are crucial for the ATP-site recognition and binding: H-bonding, hydrophobic, and $\pi-\pi$ interaction.[15,16] With the exception of the hydrophobic one, these interactions can be approximated in terms of electrostatic and van der Waals (short-range repulsion and dispersion) enthalpic contributions. Because of the long-range nature of electrostatic interactions, these were considered beyond simply their contribution to H-bonding.

Calculations were performed to generate a set of quantum chemical and classical descriptors relevant to each of these interactions as discussed below. Potential steric issues resulting from the larger relative size of template **2** were ignored, since they could not be treated by these calculations.

Electrostatics. The electrostatic complementarity is determined by a favorable matching of the electrostatic features on buried surfaces of the binding molecules, which are responsible for the H-bonding and salt-bridge interactions. It plays a crucial role in ligand recognition of the kinase ATP-binding site. At the same time, the water medium is by far the best medium for the favorable electrostatic interaction both with a ligand and with a protein. As a result, a strong ligand−protein electrostatic interaction would contribute to the binding free energy only by minimization of the desolvation penalties.[16] For this reason, the electrostatic properties of the proposed templates **3**−**5** were evaluated relative to those of the known active ligands **1** and **2**, as well as to water. A separation of the ligand−protein electrostatic interactions into close- and long-range contributions was adopted for the analysis. For close contacts, the H-bonding capacities of the ligand were expected to best match those of the water molecules. The electrostatic long-range behavior of the ligand should be evaluated relative to the corresponding properties of the water molecules displaced by the ligand in the active site.

The molecular electrostatic potential (MEP) associated with acceptor or donor atoms is a simple measure of the H-bonding capacity of the molecules.[17−20] As shown in Figure 3 the negative MEP surface is concentrated at the terminal heteroatom(s) of each ring system. Interestingly, the triazoles and benzisoxazoles show an uneven distribution of electron density on one of the two adjacent heteroatoms, which is reflected in the values of the corresponding atomic charges fitted to MEP (ESP charges, Table 1). Among all acceptors considered in this study, the oxygen of the isolated water molecule has the highest effective charge, which is comparable in magnitude with the total charge of the nitrogen acceptors of the triazolopyridine.

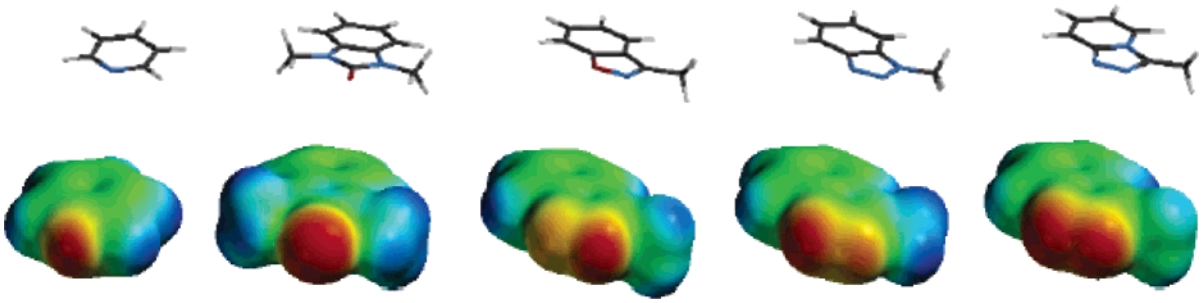

Figure 3. Molecular electrostatic potentials of the H-bond fragments (Figure 2) on the 0.002 au isodensity surface. The potentials are calculated at the B3LYP/6-311G(d,p) level of theory and shown with identical chromatic scales (red is more negative, greater electron density; blue is more positive, less electron density).

Table 1. Calculated Molecular and Atomic Properties

compound	ESP charges	μ, D	μ/V, D/Å^3	ΔG_{solv}, kcal/mol	log*P*	ASA-H (Å^2)	η (eV)
1 pyridine	N, −0.62	2.20	0.026	−5.2	0.73	108.2	5.78
2 benzoimidazolone	O, −0.53	2.13	0.013	−6.7	1.46	311.7	5.06
3 benzoisoxazole	O, −0.17 N, −0.37	3.17	0.024	−5.6	2.09	239.6	5.57
4 benzotriazole	N3[a], −0.38 N2[a], −0.21	4.09	0.031	−8.3	1.06	206.5	5.50
5 triazolopyridine	N3[a], −0.44 N2[a], −0.32	5.54	0.043	−11.9	0.94	187.4	5.23
6 water	O, −0.74	2.07	0.107	−7.3			

[a] Numbered to be consistent with compounds **20** and **25**.

The long-range behavior of a ligand MEP contributes to the interaction with remote areas of the kinase. It can be mathematically presented by expansion over the electrostatic moments (the multipole expansion).[21,22] In the case of the neutral molecules, the molecular dipole moment, $\boldsymbol{\mu}$, describes the major contribution to the long-range electrostatic interactions. The calculated dipole moments for the templates are listed in Table 1. All dipole moments are approximately parallel to each other (not shown) and describe directionality of the binding to the ATP site; this is an important factor in the ligand/kinase molecular recognition. The contribution of these dipole moments to the overall binding free energies should be evaluated relative to the sum of the dipole moments of the water molecules displaced by the templates **1**−**5** in the cavity. This allows for the introduction of an approximate correction for the actual binding site desolvation penalty. This correction depends on the molecular van der Waals volume, *V*, which varies for the fragments considered in the current study. In the simplest case, the dipole moments of the displaced waters are uniformly aligned along the $\boldsymbol{\mu}$ of the template. Despite the obvious simplification, this allows for the harmonization of all the dipole values to one scale by calculating μ/V descriptors (Table 1). For the fragments under consideration, this property is the highest for the triazolopyridine (0.043 D/Å^3) and the benzotriazole (0.031 D/Å^3), demonstrating that the triazoles have the most favorable long-range electrostatic properties for binding. At the same time, the μ/V value of 0.107 D/Å^3 for the water molecule reflects the superior capacity of the aqueous medium for attractive electrostatic interactions.

The electrostatic descriptors considered thus far reflect the properties of the free unperturbed molecules. However, polarization of the molecular charge density is an additional phenomenon, which needs to be considered with respect to the ligand/protein electrostatic interaction. It takes place upon binding as a response on the external electric field **F** imposed by the unperturbed kinase. This leads to the formation of induced molecular dipole moment, $\Delta\boldsymbol{\mu}$, which contributes to the attractive electrostatic interaction with the kinase. The above considerations for the molecular dipole moment $\boldsymbol{\mu}$ are also applicable to the $\Delta\boldsymbol{\mu}$. This moment can be approximated as $\Delta\boldsymbol{\mu} = {}^1/_2\alpha\mathbf{F}$, [22] where α is a molecular polarizability. Since α is linearly correlated with the molecular volume,[23] the α/V values are quite similar for all the ligands under consideration and are equal to ∼0.10 at the B3LYP/6-311G(d,p) level of theory. Since the field **F** is also considered to be fixed for a given protein conformation, $\Delta\mu/V$ should be a uniform property for all the ligands.

Thus, with respect to the overall electrostatic properties in water, the benzotriazole and triazolopyridine display superior characteristics, which are crucial for the recognition component of binding. On the other hand, the calculated solvation energies are also the highest for these ligands (Table 1), which correspond to the higher penalties to be paid upon ligand desolvation in the active site.

Hydrophobic Interaction. Molecular recognition due to the hydrophobic interactions is determined by shape matching and lipophilic (hydrophobic) complementarity. In contrast to the electrostatics, the hydrophobic interaction with the binding site introduces the major contribution to the binding free energy.[16] This interaction at room temperature is believed to be entropy-driven due to reorganization of water molecules at the interface with the hydrophobic (nonpolar) surfaces.[24,25] The hydrophobic interaction capacity can be evaluated by the water-accessible hydrophobic surface area of the molecule,[25] ASA-H, and the octanol−water partitioning coefficient, logP_{ow}.[26] The corresponding properties are shown in Table 1. Based on both descriptors, the highest hydrophobicity was found for the benzimidazolone and benzoisoxazole and the lowest one for pyridine. The triazole templates display comparable

hydrophobic parameters, the benzotriazole being somewhat more hydrophobic.

$\pi-\pi$ **Interactions.** This is an attractive medium-range interaction between aromatic (π-electron) molecular fragments, which takes its origin from dispersion and electrostatic forces.[27] These same fragments also usually contribute to the hydrophobic interaction energy with the binding site. The molecular recognition due to $\pi-\pi$ interactions is determined by the orientation priorities of the interacting fragments, which are dictated by the intermolecular electrostatic forces. The strength of the $\pi-\pi$ attraction is predominantly determined by dispersion interactions[27] and thus by a degree of aromaticity of the ligand. The latter property can be evaluated by absolute chemical hardness, η, as approximated by using Koopmans' theorem: $\eta = (\text{LUMO} - \text{HOMO})/2$.[28] Here HOMO and LUMO are, respectively, energies of the highest occupied and lowest unoccupied molecular orbitals. The highest aromaticity (η) was found for the pyridine and benzoisoxazole molecules, followed by the benzotriazole and triazolopyridine.

Once the computational evaluation of the various fragments was completed, the challenge was to use this information to identify those potentially superior to the benzimidazolone **2**. Although it is possible to rank the fragments according to their hydrophobic and $\pi-\pi$ interaction capacities in the order of benzoisoxazole > benzotriazole > triazolopyridine and in the opposite order for their electrostatic properties, it is their combined effect on the free energy of binding that is meaningful. The hydrophobic and $\pi-\pi$ interaction properties should predominate in determining the binding potency.[16] As compared to the benzimidazolone **2**, the three proposed fragments should be reasonable substitutes since they all have superior $\pi-\pi$ interaction capacities balanced by reduced capacities for hydrophobic interactions. Ultimately, the ability of these fragments to replace the benzimidazolone group would require experimental follow-up.

Synthesis of Kinase Inhibitors

In contemplating the experimental evaluation of the proposed atypical kinase templates, we planned to incorporate these fragments into inhibitors within a constant framework and determine their biological activity in a p38α enzyme inhibition assay. The benzoisoxazole fragment was eliminated from synthetic consideration because any eventual inhibitor incorporating this group would be more lipophilic (thus potentially more metabolically unstable) than the compounds it was designed to replace. Since in vitro microsomal stability was frequently problematic for the benzimidazolone series, we had little interest in compounds potentially less stable. The constant framework chosen for the remaining compounds was 4-(4-fluoro-phenyl)-oxazole. While it is known [12] that using oxazole as the central ring is not optimal for potency verses p38α, it does eliminate the H-bond donor capacity and tautomer ambiguity associated with using an imidazole core. The final consideration was with the connectivity of the proposed H-bond acceptor with the central oxazole ring and the nature of any substituent. Previous work in our labs on benzimidazolone analogues indicated that a highly favorable substitution pattern is isopropyl, methyl with the connection to the central ring at C5 (see **15** in Scheme 2 for numbering). However, based on the localization of the electron density on N3 of the benzotriazole system, modeling relative to the benzimidazolone suggested that the better point of attachment for the triazoles would be at C6 rather than C5 (see **20** in Scheme 3 for numbering). For consistency, isopropyl was chosen as the substituent for the benzotriazole fragment. The triazolopyridine was matched to the benzotriazole, and the pyridine analogue was used as a reference agent to archetypal pyridyl-imidazole p38 inhibitors.

Scheme 1. Synthesis of Pyridine Derivative[a]

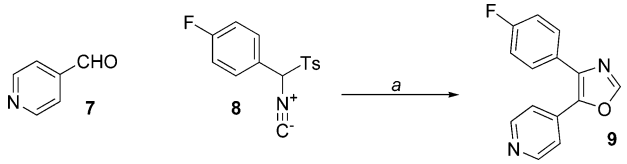

[a] Reagents and conditions: (a) K_2CO_3, acetonitrile, 22 °C, 2 h, then 70 °C, 18 h, 60%.

Scheme 2. Synthesis of Benzimidazolone Derivative[a]

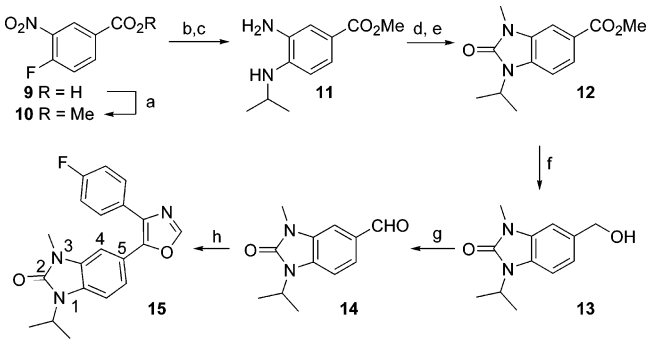

[a] Reagents and conditions: (a) oxalyl chloride, cat. *N,N*-dimethylformamide, CH_2Cl_2, 22 °C, 16 h, then Et_3N, MeOH, 22 °C, 16 h, 96%; (b) isopropylamine, CH_2Cl_2, 22 °C, 2 h, 91%; (c) H_2, Pd/C, 22 °C, 1 h, 100%; (d) phosgene, PhMe/CH_2Cl_2, 22 °C, 16 h, 56%; (e) NaH, dimethyl sulfoxide, 22 °C, 1 h, then MeI, 22 °C, 48 h, 63%; (f) $LiBH_4$, THF, MeOH 80 °C, 18 h, 67%; (g) TEMPO, *N*-chlorosuccinimide, tetrabutylammonium chloride, pH = 8.6 buffer, CH_2Cl_2, 22 °C, 16 h, 68%; (h) **8**, K_2CO_3, acetonitrile, 22 °C, 2 h, then 50 °C, 36 h, 11%.

Scheme 3. Synthesis of Benzotriazole Derivative[a]

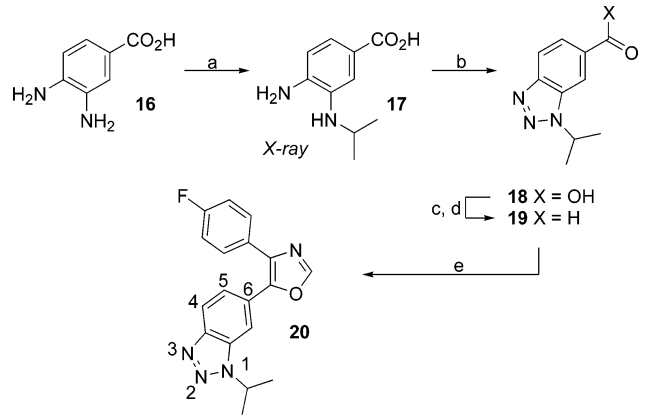

[a] Reagents and conditions: (a) acetone, AcOH, THF/*N,N*-dimethylformamide, 2 h, 22 °C, then $NaBH(OAc)_3$, 2.5 h, 36%; (b) 6 N HCl, aqueous $NaNO_2$, 0 °C, 1 h, 79%; (c) oxalyl chloride, CH_2Cl_2, cat. *N,N*-dimethylformamide, 22 °C, 4 h, then $(i\text{-Pr})_2NEt$, NHMeOMeHCl, 22 °C, 16 h, 77%; (d) DIBAL-H, PhMe, −78 to 0 °C, 1.5 h, 67%; (e) **8**, K_2CO_3, CH_3CN, 22 °C, 4 h, then 70 °C, 14 h, 62%.

Scheme 4. Synthesis of Triazolopyridine Derivative[a]

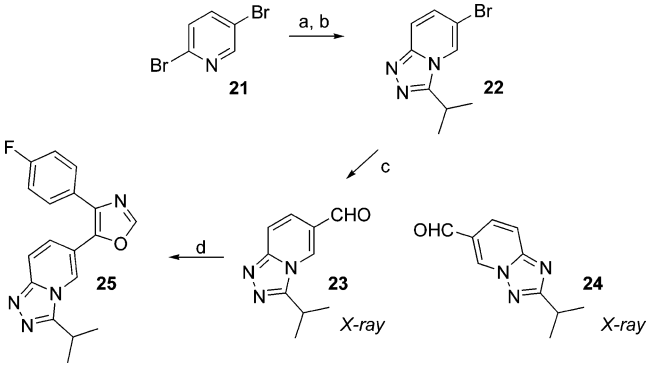

[a] Reagents and conditions: (a) hydrazine hydrate, PEG/2-butanol/water, 98 ° C, 29 h, 87%; (b) isobutyryl chloride, reflux, 3 h, then NaOH freebase, 74%; (c) *i*-PrMgCl, THF, −6 to 6 °C, 0.5 h, then *N,N*-dimethylformamide, reflux, 3 h, 78%; (d) **8**, K_2CO_3, CH_3CN, 22 °C, 16 h, then 70 °C, 24 h, 98%.

The syntheses of the four compounds used in the comparison are shown in Schemes 1−4. As shown in Scheme 1, the known pyridine analogue was prepared in a single step[29−31] from commercially available 4-pyridylcarboxaldehyde.

As shown in Scheme 2, the synthesis of the benzimidazolone **15** starts from commercially available 4-fluoro-3-nitrobenzoic acid by esterification, reaction with isopropylamine, and hydrogenation to give **11** in 87% overall yield. Imidazolone ring formation with phosgene and alkylation with methyl iodide gave the benzimidazolone intermediate **12** in 30% yield. Reduction with lithium borohydride and *N*-chlorosuccinimide/TEMPO oxidation [32] gave the aldehyde **14** in 45% yield. Finally, reaction of **14** with **8** gave **15** in poor yield as result of the need to balance the thermal requirement for [3 + 2] reaction and the decomposition of the isonitrile under the conditions.

The synthesis of the benzotriazole starts with the selective reductive amination of 3,4-diaminobenzoic acid with acetone, exploiting the difference in reactivity of the amines due the presence or absence of conjugation with the carboxylic acid (see Scheme 3). The regiochemistry of reaction was confirmed by X-ray crystallographic analysis of **17**. Reaction of **17** with sodium nitrite and hydrochloric acid cleanly gave the benzotriazole acid **18**. Conversion of the acid **18** to the Weinereb amide followed by DIBAL-H reduction gave the aldehyde **19** in 51% yield. The target compound was again prepared by reaction of the aldehyde with **8**; this time the better yield is presumed to arise from the ability of the [3 + 2] intermediate adduct to form without heating. Subsequent elimination of the sulfinic acid requires heating.

Finally, the triazolopyridine **25** (CP-808844) was assembled as shown in Scheme 4. Reaction of hydrazine and 2,5-dibromopyridine in aqueous 2-butanol−PEG mixture followed by acylation and cyclodehydration in neat isobutyryl chloride gave the bromo triazolopyridine **22**. The transformation of the bromide to the aldehyde went smoothly to the desired aldehyde **23** by Grignard exchange[33] followed by reaction with *N,N*-dimethylformamide provided that the workup conditions were neither too basic nor acidic. Under aqueous workup conditions that strayed significantly from pH 7, complete Dimroth-like rearrangement[34,35] of the aldehyde **23** to **24** occurs. The structure of each isomer was confirmed by X-ray crystallographic determination. Reaction of the aldehyde **23** as before gave **25** in 98% yield.

Table 2. p38α Enzyme Inhibition Results

compound	p38α IC_{50} (nM)	*n*/SD (nM)	$\Delta\Delta G/N$ (kcal/mol)[a]
9	1460	5/345	0.44
15	30	9/3.5	0.40
20	0.9	10/0.1	0.51
CP-808844 **25**	5.0	18/0.5	0.47

[a] $\Delta\Delta G = -RT \ln(IC_{50})$; *N* is the number of non-hydrogen atoms.

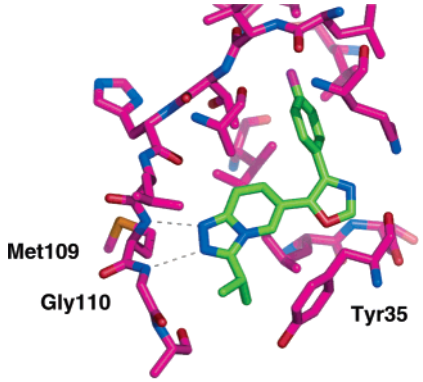

Figure 4. X-ray structure of **25** bound to p38α.

Results and Discussion

With the synthesis complete, the compounds were evaluated in a p38α isolated enzyme assay (see Table 2).[12] Although the pyridyl analogue **9** is known,[29−31] the p38α activity has not been reported, and **9** was included as a reference agent to put the activity of the other three compounds into perspective. The most appropriate comparisons can be made between the triazole analogues **20** and **25** and with the benzimidazolone **15** after which they were conceived. The superior potency of the triazoles relative to the benzimidazolone **15** eliminated our initial concerns about their dual atom H-bond acceptor capacity, but confirmation of the binding mode was not obtained until the X-ray structure determination of a complex between p38α and **25** was achieved.[36] As shown in Figure 4, this revealed that both triazole nitrogens serve as H-bond acceptors as a result of movement of the crossover connection residues, which allows Gly110NH, in addition to Met109NH, to participate as an H-bond donor. Similar movement has been seen recently with other p38 inhibitors;[10,37] however, to our knowledge this represents the first example of a kinase inhibitor where two distinct atoms act as H-bond acceptors with the crossover connection region. In light of these results, it is also likely that the carbonyl group in the benzimidazolone **15** acts as a dual H-bond acceptor as is seen with other carbonyl-containing p38 inhibitors.[10]

In terms of making comparisons between **9**, **15**, **20**, and **25** beyond strictly potency as a way of prioritizing follow-up work, it is possible to crudely evaluate their binding efficiencies without regard for potential differences in binding mode or steric interactions.[39,40] One simple ligand evaluation method can be performed using the maximum ligand affinity scale.[40] For this, the IC_{50}

values are converted to the free energy of binding as $\Delta\Delta G = -RT \ln(IC_{50})$. All ligands, except **9**, fit the $\Delta\Delta G$ dependence for the number of non-hydrogen atoms, N, determined for a wide range of the tight-binding ligands. Comparison of the ligands was performed in terms of the free energy of binding per heavy atom, $\Delta\Delta G/N$ (Table 2).[40] The higher this property the more efficiently the non-hydrogen atoms drive the affinity. In agreement with the IC_{50} data, the highest $\Delta\Delta G/N$ values were found for the triazole-based ligands. These data also suggest that the smallest ligand, **9**, is more efficient than the largest one, **15**. This observation seems to indicate that **9** is favorable for further optimization, but given its absolute potency, it is not clear that this compound would be a better choice than the triazoles.

In terms of actually trying to understand the potency outcome and which calculated properties were the most predictive, the situation is more complex. While the MEP alone correctly predicted the trend in potency for a series of compounds reported by Johnson & Johnson,[19,20] the triazole examples herein highlight the need to also evaluate the capacity for hydrophobic and $\pi-\pi$ interactions. The superior electrostatic properties (higher H-bonding capacity and higher μ/V, Figure 3, Table 1) notwithstanding, the triazolopyridine **25** is less potent than the benzotriazole **20**. This observation is consistent with the fact that H-bond and electrostatic interactions generally do not contribute much to the overall free energy of binding as a result of the trade offs with desolvation.[16] On the other hand, the potency of the two triazoles can be correctly ranked by their capacity for hydrophobic and $\pi-\pi$ interactions (Table 1). These types of interactions are especially important given the conformational changes of the activation loop upon ligand binding with the Tyr35 side-chain "closing" down on the binding site (Figure 4).[9] The resulting "T-shaped" orientation of the tyrosine phenol and the pyridine ring of **25** is not far from the ideal for $\pi-\pi$ interactions: the distance between ring centers is 5.9 Å in comparison with 5.0 Å for the corresponding benzene dimer at equilibrium.[27] Even at this distance, there is an important attractive contribution for the $\pi-\pi$ interaction energy between benzene molecules estimated at about 1.5 kcal/mol.[27] With respect to the potency of the triazoles relative to the benzimidazolone **15**, the superior electrostatic properties of the triazole may contribute, but more likely there are steric constraints that prevent **15** from reaching its full potential. The latter interpretation is consistent with the observation that the benzimidazolone **15** displays the lowest $\Delta\Delta G/N$ value among all the ligands under consideration (Table 2).

Conclusion

In this work, we set out to use a set of computationally derived descriptors to evaluate a series of heterocyclic fragments for their possible use in atypical kinase inhibitors. In the end, we were able to identify significantly more potent compounds that at the same time have superior calculated physicochemical properties than the benzimidazolone group that they were designed to replace. While a complex interplay exists between the calculated parameters used, descriptors for hydrophobic and $\pi-\pi$ interaction capacities were the most useful in ranking the potency.

Computational Details

The geometries of the five fragments were fully optimized in the gas phase at the B3LYP/6-31G(d) level of theory. The molecular dipole moments, isotropic polarizabilities, and atomic charges were evaluated by single-point calculations at the B3LYP/6-311G(d,p) level. The ESP atomic charges were calculated according to the CHELPG algorithm.[41] The polarized continuum model (PCM)[42,43] was adopted at the HF/6-31+G(d) level of theory for the geometry optimizations in water, followed by single-point calculation of the solvation free energy, ΔG_{solv}, and absolute chemical hardness, η, descriptors. The majority of the quantum chemical calculations were performed by the Gaussian98/03 program suites.[44] The molecular electrostatic potentials were calculated at the B3LYP/6-311G(d,p) level of theory and plotted using Spartan'02 software.[45]

The octanol−water partition coefficients, log$P$, were predicted using ACD/labs 6.00 software package.[46] The van der Waals molecular volume, V, and water-accessible hydrophobic surface area, ASA-H, descriptors were evaluated by the MOE software.[47] Only atoms with absolute values for the ESP atomic charges of less than 0.2 e^- were considered in calculating the ASA-H. The molecular geometries optimized in solution were adopted for these calculations.

Experimental Section

Melting points were determined using a Büchi B-545 melting point apparatus and are uncorrected. ^{1}H NMR spectra were obtained using a Varian Unity 400 or 500 MHz. Chemical shifts are reported in parts per million (δ) relative to residual chloroform (7.24 ppm), dimethyl sulfoxide (2.49 ppm), or methanol (3.30 ppm) as an internal reference. Coupling constants (J) are reported in hertz (Hz). The peak shapes are denoted as follows: s, singlet; d, doublet; t, triplet; m, multiplet; br, broad. APcI mass spectra were recorded by direct flow analysis for positive and negative atmospheric pressure chemical ionization (APcI) scan modes using a Waters APcI/MS model ZMD mass spectrometer equipped with Gilson 215 liquid handling system. GCMS mass spectral data were obtained using the electron impact ionization technique of the parent molecular mass using a Hewlett-Packard 6890 series GC system equipped with a Hewlett-Packard 5973 mass selective detector. LCMS molecular weight identification was recorded by positive and negative electrospray ionization (ESI) scan modes using a Waters/Micromass ESI/MS model ZMD/LCZ mass spectrometer equipped with Gilson 215 liquid handling system and Hewlett-Packard 1100 diode array detector. Small-molecule X-ray structures were collected on a Bruker APEX or a Siemens P4 diffractometer. Normal-phase silica gel flash chromatography was performed using Biotage Flash40 or 25 systems. Reverse-phase purification was conducted with a Waters 600 system with a 486 tunable detector. Elemental analyses were performed at Quantitative Technologies Inc., Whitehouse, NJ. The term "concentrated" refers to the removal of solvent under reduced pressure using a rotory evaporator.

4-[4-(4-Fluorophenyl)-5-oxazolyl]-pyridine (9).[29,31] To a stirred solution of 4-pyridinecarboxaldehyde (0.53 g 5.0 mmol) in 10 mL of acetonitrile was added α-(*p*-toluensulfonyl)-4-fluorobenzylisonitrile (1.45 g, 5.0 mmol) followed by potassium carbonate (0.9 g, 6.5 mmol). The mixture was stirred at 22 °C for 2 h and at 70 °C for 16 h. The mixture was cooled to 22 °C, diluted with water, and extracted with methylene chloride. The organic extracts were dried over sodium sulfate and filtered. The filtrate was concentrated, and the crude solid was purified by flash chromatography, eluting with ethyl acetate and hexanes (1:1) to give 0.73 g (60%) of 4-[4-(4-fluorophenyl)-5-oxazolyl]-pyridine[29,31] as a white solid. LCMS (*m/z*): 241 (M + H). ^{1}H NMR (400 MHz, $CDCL_3$): δ 8.60 (dd, J = 4.6, 1.7

Hz, 2 H), 8.00 (s, 1 H), 7.60 (m, 2 H), 7.46 (dd, $J = 4.6$, 1.7 Hz, 2 H), 7.12 (m, 2 H).

4-Fluoro-3-nitrobenzoic Acid Methyl Ester (10). To a stirred solution of 4-fluoro-3-nitrobenzoic acid (50.0 g, 0.27 mol) in 500 mL of methylene chloride was added 1 mL of *N,N*-dimethylformamide, followed by oxalyl chloride (26 mL, 0.30 mol), and the mixture was stirred at 22 °C for 16 h. The yellow solution was concentrated to a yellow semisolid and used in the subsequent step.

To a stirred solution of the crude acid chloride in 200 mL of methylene chloride was added dropwise a mixture of 74 mL of triethylamine and 86 mL of methanol. The mixture was stirred for 16 h at 22 °C and diluted with aqueous sodium bicarbonate, and the layers were separated. The organic phase was washed with saturated aqueous bicarbonate (3×), water (1×), and brine (1×) and dried (Na_2SO_4) and filtered. The filtrate was concentrated to a yellow oil, which solidified to give 52.4 g (96%) of 4-fluoro-3-nitrobenzoic acid methyl ester as a yellow solid. ^{1}H NMR (400 MHz, $CDCl_3$): δ 8.72 (dd, $J =$ 8. 0, 2.1 Hz, 1 H), 8.30 (d, $J =$ 8. 7, 4.2, 2.1 Hz, 1 H), 7.37 (dd, $J = 10.3$, 8.7 Hz, 1 H), 3.96 (s, 3 H). Anal. Calcd for $C_8H_6FNO_4$: C, 48.25; H, 3.04; N, 7.03. Found: C, 48.27; H, 2.83; N, 6.89.

3-Amino-4-isopropylaminobenzoic Acid Methyl Ester (11). To a stirred, cold (0 °C) solution of 4-fluoro-3-nitrobenzoic acid methyl ester (5.0 g, 25.1 mmol) in 80 mL of methylene chloride was added isopropylamine (4.2 mL, 49.7 mmol). The cold bath was removed after 3 h, and the mixture was stirred at 22 °C for 2 h. The mixture was diluted with water and extracted with methylene chloride (3×). The combined organic extracts were washed with water and brine, dried (Na_2SO_4), and filtered. The filtrate was concentrated to give 5.5 g (91%) of 4-isopropylamino-3-nitrobenzoic acid methyl ester as a yellow solid.

A mixture of 4-isopropylamino-3-nitrobenzoic acid methyl ester (4.5 g, 18.9 mmol), 60 mL of ethanol, and palladium on carbon (0.25 g) was shaken under a 40 psi atmosphere of hydrogen gas for 1 h. The mixture was filtered through nylon and concentrated to give 3.9 g (100%) of 3-amino-4-isopropylaminobenzoic acid methyl ester as an off-white solid. LCMS (*m/z*): 209 (M + H). ^{1}H NMR (400 MHz, $CDCl_3$): δ 7.56 (d, J = 8.3 Hz, 1 H), 7.39 (s, 1 H), 6.58 (d, $J =$ 8.3 Hz, 1 H), 3.83 (s, 3 H), 3.67−3.70 (m, 1 H), 1.24 (d, $J =$ 6.6 Hz, 6 H). Anal. Calcd for $C_{11}H_{16}N_2O_2$: C, 63.44; H, 7.74; N, 13.45. Found: C, 63.19; H, 7.47; N, 13.09.

1-Isopropyl-3-methyl-2-oxo-2,3-dihydro-1*H*-benzoimidazole-5-carboxylic Acid Methyl Ester (12). To a stirred solution of 3-amino-4-isopropylaminobenzoic acid methyl ester (3.7 g, 17.8 mmol) in 50 mL of methylene chloride was added phosgene (9.4 mL, 20% in toluene) dropwise. The mixture was stirred at 22 °C for 16 h; the reaction was quenched with saturated aqueous bicarbonate, and the mixture was extracted with methylene chloride (3×). The combined organic extracts were washed with water and brine, dried (Na_2SO_4), and filtered. The filtrate was concentrated to give a tan solid. This material was suspended in a mixture of 8 mL of hexanes, 1 mL of ethyl acetate, and 0.5 mL of methylene chloride and stirred for 16 h at 22 °C. The suspension was filtered, and the solids were collected and dried to give 2.35 g (56%) of 1-isopropyl-2-oxo-2,3-dihydro-1*H*-benzoimidazole-5-carboxylic acid methyl ester as a white solid. To a stirred solution of 1-isopropyl-2-oxo-2,3-dihydro-1*H*-benzoimidazole-5-carboxylic acid methyl ester (0.54 g, 2.3 mmol) in 5 mL of dimethyl sulfoxide was added sodium hydride (60%, 0.11 g, 2.8 mmol). The resulting mixture was stirred for 1 h at 22 °C before methyl iodide (0.3 mL, 4.6 mmol) was added. The mixture was stirred for 48 h at 22 °C; the reaction was quenched with water, and the mixture was extracted with methylene chloride (3×). The combined organic layers were washed with water and brine, dried (Na_2SO_4), and filtered, and the filtrate was concentrated to give 0.65 g of a yellow solid. This material was purified by flash chromatography, eluting with 3:2 hexanes/ethyl acetate to give 0.36 g (63%) of 1-isopropyl-3-methyl-2-oxo-2,3-dihydro-1*H*-benzoimidazole-5-carboxylic acid methyl ester as a white solid. LCMS (*m/z*): 249 (M + H). ^{1}H NMR (400 MHz, $CDCl_3$): δ 7.81 (d, $J =$ 8.3 Hz, 1 H), 7.64 (s, 1 H), 7.12 (d, $J =$ 8.3 Hz, 1 H), 4.69−4.76 (m, 1 H), 3.91 (s, 3 H), 3.43 (s, 3 H), 1.52 (d, $J = 7.0$ Hz, 6 H). Anal. Calcd for $C_{13}H_{16}N_2O_3$: C, 62.89; H, 6.50; N, 11.28. Found: C, 62.82; H, 6.47; N, 11.34.

5-Hydroxymethyl-1-isopropyl-3-methyl-1,3-dihydrobenzoimidazol-2-one (13). To a stirred solution of 1-isopropyl-3-methyl-2-oxo-2,3-dihydro-1*H*-benzoimidazole-5-carboxylic acid methyl ester (10.5 g, 42.3 mmol) in 140 mL of tetrahydrofuran was added lithium borohydride (1.84 g, 84.6 mmol) at 22 °C. The mixture was heated to 80 °C, and methanol (6.8 mL, 16.9 mmol) was added dropwise with gas evolution. The resulting mixture was heated at 80 °C for 18 h before being cooled to 22 °C. The hazy mixture was diluted with saturated sodium bicarbonate and extracted with methylene chloride (4×). The combined organic extracts were washed with water and brine, dried over sodium sulfate, and filtered. The filtrate was concentrated to give 6.27 g (67%) of 5-hydroxymethyl-1-isopropyl-3-methyl-1,3-dihydro-benzoimidazol-2-one as a white solid. LCMS (*m/z*): 221 (M + H). ^{1}H NMR (400 MHz, $CDCl_3$): δ 7.01−7.10 (m, 3 H), 4.68−4.75 (m, 3 H), 3.33 (s, 3 H), 1.50 (d, $J =$ 7.0 Hz, 6 H). Anal. Calcd for $C_{12}H_{16}N_2O_2$: C, 65.43; H, 7.32; N, 12.72. Found: C, 65.29; H, 7.43; N, 12.55.

1-Isopropyl-3-methyl-2-oxo-2,3-dihydro-1H-benzoimidazole-5-carbaldehyde (14). To a stirred solution of 5-hydroxymethyl-1-isopropyl-3-methyl-1,3-dihydro-benzoimidazol-2-one (8.1 g, 36.8 mmol) in 200 mL of methylene chloride was added in the following order: TEMPO (1.7 g, 11.0 mmol), tetrabutylammonium chloride (3.1 g, 11.0 mmol), *N*-chlorosuccinimide (9.3 g, 69.9 mmol), and 400 mL of pH 8.6 buffer ($NaHCO_3$−K_2CO_3).[32] The resulting mixture was stirred at 22 °C for 18 h. The layers were separated, and the aqueous layer was extracted with methylene chloride (3×). The combined organic extracts were washed with aqueous sodium bicarbonate (1×), water (1×), and brine (1×), dried (Na_2SO_4), and filtered, and the filtrate was concentrated to a dark yellow solid. The material was purified by flash chromatography, eluting with 2:1 hexanes/ethyl acetate to give 5.5 g (68%) of 1-isopropyl-3-methyl-2-oxo-2,3-dihydro-1*H*-benzoimidazole-5-carbaldehyde as a white solid. LCMS (*m/z*): 219 (M + H). ^{1}H NMR (400 MHz, $CDCl_3$): δ 9.92 (s, 1 H), 7.58 (dd, $J =$ 8.3, 1.7 Hz, 1 H) 7.51 (s, 1 H), 7.21−7.25 (m, 1 H), 4.71−4.78 (m, 1 H), 3.44 (s, 3 H), 1.54 (d, $J = 7.0$ Hz, 6 H). Anal. Calcd for $C_{12}H_{14}N_2O_2$: C, 66.04; H, 6.47; N, 12.84. Found: C, 65.99; H, 6.23; N, 12.80.

5-[4-(4-Fluoro-phenyl)-oxazol-5-yl]-1-isopropyl-3-methyl-1,3-dihydrobenzoimidazol-2-one (15). To a stirred suspension of 1-isopropyl-3-methyl-2-oxo-2,3-dihydro-1*H*-benzoimidazole-5-carbaldehyde (0.20 g, 0.92 mmol) in 3 mL of acetonitrile was added α-(*p*-toluensulfonyl)-4-fluorobenzylisonitrile (0.53 g, 1.8 mmol) and powdered potassium carbonate (0.25 g, 1.8 mmol). The mixture was heated at 50 °C for 18 h before adding another equivalent each of α-(*p*-toluensulfonyl)-4-fluorobenzylisonitrile (0.26 g, 0.92 mmol) and potassium carbonate (0.13 g, 0.92 mmol). The mixture was heated at 50 °C for an additional 18 h. The mixture was cooled to 22 °C, diluted with water, and extracted with ethyl acetate (3×). The combined organic extracts were washed with water and brine, dried (Na_2SO_4), and filtered, and the filtrate was concentrated to a dark yellow solid. This material was purified by flash chromatography, eluting with 3:2 hexanes/ethyl acetate to give 0.2 g of an off-white foam. This material was further purified by reverse-phase HPLC (MS C_{18} Xterra 5 μm, 30 mm × 100 mm; 42 mL/min; 214 nM detection), eluting from 6:4 water/acetonitrile to 2:8 water/acetonitrile (with 0.1% TFA) over 10 min. The desired material had a retention time of 6.3 min. This material was taken-up in ethyl acetate and washed with aqueous sodium bicarbonate (1×), water, and brine, dried (Na_2SO_4), and filtered, and the filtrate was concentrated to give 100 mg of a white foam. Final purification was then achieved by flash chromatography, eluting with 55:45 hexanes/ethyl acetate to give 36 mg (11%) of 5-[4-(4-fluoro-phenyl)-oxazol-5-yl]-1-isopropyl-3-methyl-1,3-dihydrobenzoimidazol-2-

one as a white solid. LCMS (*m/z*): 352 (M + H). ^{1}H NMR (500 MHz, $CDCl_3$): δ 7.98 (s, 1 H), 7.67−7.70 (m, 2 H), 7.28−7.31 (m, 1 H), 7.19 (d, J = 1.6 Hz, 1 H), 7.08−7.14 (m, 3 H), 4.73−4.79 (m, 1 H), 3.38 (s, 3 H), 1.56 (d, J = 6.7 Hz, 6 H). Anal. Calcd for $C_{20}H_{18}FN_3O_2$: C, 68.36; H, 5.16; N, 11.96. Found C, 68.17; H, 4.93; N, 11.56.

4-Amino-3-isopropylaminobenzoic Acid (17). To a stirred solution of 3,4-diaminobenzoic acid (25.0 g, 0.16 mol) in 300 mL of tetrahydrofuran and 45 mL of *N,N*-dimethylformamide was added 12 mL (0.16 mol) of acetone and 9.4 mL of acetic acid. The mixture was stirred at 22 °C for 2 h before sodium triacetoxyborohydride (41.8 g, 0.20 mol) was added portionwise. The resulting mixture was stirred for 2.5 h before being filtered through Celite and rinsed with tetrahydrofuran. The filtrate was concentrated to a dark oil, which was mixed with water to give a tan precipitate. The solids were collected by vacuum filtration, suspended in a mixture of diisopropyl ether, methanol, and ethyl acetate, and stirred at 22 °C for 16 h. The solids were collected by vacuum filtration, and rinsed with ethyl acetate and water to give after drying 11.7 g (36%) of 4-amino-3-isopropylaminobenzoic acid as an off-white solid (discolors over time), which was crystallized for X-ray determination by slow evaporation from ethyl acetate and hexanes; mp = 151.8−152.1 °C. ^{1}H NMR (500 MHz, $CDCl_3$): δ 7.55 (d, J = 7.7 Hz, 1 H), 7.44 (s, 1 H) 6.72 (d, J = 7.7 Hz, 1 H), 3.65−3.70 (m, 1 H), 1.26 (d, J = 6.2 Hz, 6 H). Anal. Calcd for $C_{10}H_{14}N_2O$: C, 61.84; H, 7.27; N, 14.42. Found C, 61.76; H, 7.30; N, 14.34.

3-Isopropyl-3*H*-benzotriazole-5-carboxylic acid (18). To a stirred, cold (0 °C) suspension of 4-amino-3-isopropylaminobenzoic acid (11.7 g, 60.2 mmol) in 125 mL of 6 N hydrochloric acid was added dropwise a solution of sodium nitrite (6.2 g, 90.4 mmol) in 50 mL of water. The mixture was stirred for 1 h at 0 °C and filtered, and the solids were collected and rinsed with water. The solids were dried to give 9.8 g (79%) of 3-isopropyl-3*H*-benzotriazole-5-carboxylic acid as a tan solid. LCMS (*m/z*): 206 (M + H). ^{1}H NMR (500 MHz, $CDCl_3$): δ 8.47 (s, 1 H), 8.19 (d, J = 8. 3 Hz, 1 H), 8.14 (m, 1 H), 5.2 (m, 1 H), 1.81 (d, J = 6.7 Hz, 6 H). Anal. Calcd for $C_{10}H_{11}N_3O_2$: C, 58.53; H, 5.40; N, 20.48. Found: C, 58.20; H, 5.31; N, 20.40.

3-Isopropyl-3*H*-benzotriazole-5-carbaldehyde (19). To a stirred mixture of 3-isopropyl-3*H*-benzotriazole-5-carboxylic acid (1.42 g, 6.9 mmol) in 140 mL of methylene chloride and 0.015 mL of *N,N*-dimethylformamide was added oxalyl chloride (0.78 mL, 9.0 mmol) at 22 °C. The mixture became a solution after 1 h and was stirred an additional 4 h at 22 °C. *N,N*-Diisopropylethylamine (4.20 mL, 24.2 mmol) and *N,O*-dimethylhydroxylamine hydrochloride (0.88 mg, 9.00 mmol) were added, and the mixture was stirred for 16 h at 22 °C. The mixture was poured into a separatory funnel and washed with aqueous sodium hydrogen phosphate, saturated aqueous bicarbonate, 0.1 N HCl, and brine. The organic layer was dried over sodium sulfate and filtered. The filtrate was concentrated to give 1.5 g of a yellow oil. This oil was purified by flash chromatography eluting with ethyl acetate and hexanes 2:1 to give 1.32 g (77%) of 3-isopropyl-3*H*-benzotriazole-5-carboxylic acid methoxy-methyl-amide as a light yellow solid. LCMS (*m/z*): 249 (M + H). ^{1}H NMR (500 MHz, dimethyl sulfoxide-d_6): δ 8.16 (s, 1 H), 8.09 (d, J = 8.3 Hz, 1 H), 7.55 (d, J = 8.3 Hz, 1 H), 5.30 (m, 1 H), 3.56 (s, 3 H), 3.33 (s, 3 H), 1.64 (d, J = 6.7 Hz, 6 H). To a stirred, cold (−78 °C) solution of 3-isopropyl-3*H*-benzotriazole-5-carboxylic acid methoxy-methyl-amide (4.26 g, 17.2 mmol) in 20 mL of toluene was added diisobutylaluminum hydride (17.2 mL; 1 M in toluene, 17.2 mmol) dropwise under a nitrogen atmosphere. After 1.5 h, the reaction was warmed to 0 °C with an ice bath; 10 mL of 1 N HCl was slowly added; the mixture was diluted with water and extracted with ethyl acetate (3×). The combined organic extracts were washed with water and brine, dried over sodium sulfate, and filtered. The filtrate was concentrated to give a yellow oil, which was purified by flash chromatography, eluting with ethyl acetate and hexanes 1:2, to a yellow oil, which crystallized on standing to give 2.2 g (67%) of 3-isopropyl-3*H*-benzotriazole-5-carbaldehyde as light yellow solid. LCMS (*m/z*): 190 (M + H). ^{1}H NMR (400 MHz, $CDCl_3$): δ 10.17 (s, 1 H), 8.18 (d, J = 8.7 Hz, 1H), 8.12 (d, J = 1.2 Hz, 1 H), 7.88 (dd, J = 8.7, 1.2 Hz, 1 H), 5.16 (m, 1 H), 1.77 (d, J = 6.6 Hz, 6 H). Anal. Calcd for $C_{10}H_{11}N_3O$: C, 63.48; H, 5.86; N, 22.21. Found: C, 63.11; H, 5.65; N, 22.22.

6-[4-(4-Fluoro-phenyl)-oxazol-5-yl]-1-isopropyl-1*H*-benzotriazole (20). To a stirred solution of 3-isopropyl-3*H*-benzotriazole-5-carbaldehyde (0.19 g, 1.0 mmol) and α-(*p*-toluensulfonyl)-4-fluorobenzylisonitrile (0.32 g, 1.1 mmol) in 3.3 mL of acetonitrile was added powdered potassium carbonate at 22 °C. The resulting suspension was stirred for 4 h at 22 °C and for 14 h at 70 °C. The mixture was cooled to 22 °C, diluted with water, and extracted with ethyl acetate (3×). The combined organic extracts were washed with brine and dried over sodium sulfate. Filtration and concentration of the filtrate gave a yellow oil, which crystallized upon standing. The crude solid was purified by flash chromatography, eluting with ethyl acetate and hexanes (65:35), to give 300 mg of an off-white solid. Recrystallization of this material from hot ethyl acetate and hexanes gave 0.20 g (62%) of 6-[4-(4-fluoro-phenyl)-oxazol-5-yl]-1-isopropyl-1*H*-benzotriazole as a white solid. APCI MS (*m/z*): 323 (M + H). ^{1}H NMR (500 MHz, $CDCl_3$): δ 8.05 (d, J = 8.8 Hz, 1 H), 8.03 (s, 1 H) 7.81 (s, 1 H), 7.66 (m, 2 H), 7.57 (d, J = 8.8 Hz, 1 H), 7.12 (m, 2 H), 5.06 (m, 1 H), 1.72 (d, J = 6.7 Hz, 6 H). Anal. Calcd for $C_{18}H_{15}FN_4O$: C, 67.07; H, 4.69; N, 17.38. Found: C, 66.68; H, 4.50; N, 17.37.

6-Bromo-3-isopropyl[1,2,4]triazolo[4,3-*a*]pyridine (22). A mixture of 2,5-dibromopyridine (35.5 g, 150 mmol) and hydrazine hydrate (55 wt %, 85.5 mL, 1.5 mol) in poly(ethylene glycol) (average M_n ca. 300, 150 mL), 2-butanol (30 mL), and water (150 mL) was refluxed for 24 h. The solution was cooled to room temperature. Water (450 mL) was added. The resulting slurry was stirred in an ice/water bath for 1 h and filtered. The cake was washed with cold water (2 × 100 mL) and dried in a vacuum oven (35 °C) for 18 h. 5-Bromopyridin-2-yl-hydrazine (24.0 g, yield 85%) was obtained as a white needle-type crystalline solid. GCMS (*m/z*): 187 (M^+). ^{1}H NMR (400 MHz, $CDCl_3$): δ 8.14 (d, J = 2.0 Hz, 1 H), 7.55 (dd, J = 8.7, 2.0 Hz, 1 H), 6.66 (d, J = 7.7 Hz, 1 H), 5.89 (brs, 1 H), 3.65 (brs, 2 H).

A mixture of isobutyryl chloride (218 mL, 2.08 mol) and 5-bromopyridin-2-yl-hydrazine (43.4 g, 231 mmol) was stirred under reflux for 3 h. The reaction slurry was cooled to room temperature, and hexane (220 mL) was added. The slurry was stirred at room temperature for 15 min and then filtered. The cake was washed with hexane (3 × 70 mL) and dried in a vacuum oven (30 °C) for 24 h. 6-Bromo-3-isopropyl[1,2,4]-triazolo[4,3-*a*]pyridine hydrochloride (58.9 g, yield 92%) was obtained as an off-white powder. Aqueous NaOH (1 N, 86 mL) was added to a mixture of 6-bromo-3-isopropyl[1,2,4]triazolo-[4,3-*a*]pyridine hydrochloride (23.4 g, 8.46 mmol) in water (130 mL) and dichloromethane (130 mL). The biphasic mixture was stirred at room temperature for 15 min. The bottom layer was separated, and the top aqueous layer was extracted with dichloromethane (60 mL). The combined organic layers were washed with 1:1 brine−water (60 mL), dried ($MgSO_4$), and concentrated. The residual oil was recrystallized from ethyl acetate (50 mL) and hexane (200 mL). 6-Bromo-3-isopropyl-[1,2,4]triazolo[4,3-*a*]pyridine (16.5 g, yield 81%) was obtained as an off-white powder. ^{1}H NMR (400 MHz, $CDCl_3$): δ 8.06 (s, 1 H), 7.64 (d, J = 9.5 Hz, 1 H), 7.24 (d, J = 9.5 Hz, 1 H), 3.33 (m, J = 7.0 Hz, 1 H), 1.52 (d, J = 7.0 Hz, 6 H). Anal. Calcd for $C_9H_{10}BrN_3$: C, 45.02; H, 4.20; N, 17.50. Found: C, 45.05; H, 4.06; N, 17.34.

3-Isopropyl-[1,2,4]triazolo[4,3-*a*]-6-pyridinecarboxaldehyde (23). A solution of 6-bromo-3-isopropyl[1,2,4]triazolo-[4,3-*a*]pyridine (5.00 g, 20.8 mmol) in THF (low water, 50 mL) was cooled to −8 °C using an acetone/dry ice bath. A solution of isopropylmagnesium chloride in THF (2.0 M, 12.5 mL, 25 mmol) was added via a syringe over a period of 5 min. The resulting brownish slurry was stirred between −6 and 6 °C for 30 min. *N,N*-Dimethylformamide (anhydrous, 3.9 mL, 50 mmol) was added via a syringe over a period of 1 min. The cooling bath was replaced with a heating bath. The slurry was

heated to reflux and stirred under reflux for 3 h. The reaction mixture was cooled to 10 °C, and dichloromethane (100 mL) was added. The slurry was slowly poured into a stirred and cooled (15 °C) 10 wt % aqueous citric acid solution (120 mL). The biphasic mixture was stirred for 150 min. The organic layer was separated, and the aqueous layer was extracted with dichloromethane (60 mL). The combined organic extracts were washed with 1:1 v/v brine−water (30 mL), dried ($MgSO_4$), and concentrated. The brownish residual solid was recrystallized from ethyl acetate (15 mL) and hexane (15 mL). 3-Isopropyl-[1,2,4]triazolo[4,3-*a*]-6-pyridinecarboxaldehyde (3.07 g, yield 78%) was obtained as a beige powder and crystallized for X-ray determination by slow evaporation from ethyl acetate and hexanes; mp = 180.7−180.8 °C. R_f (silica gel; ethyl acetate) = 0.18. GCMS (*m/z*): 189 (M^+). ^{1}H NMR (500 MHz, $CDCl_3$): δ 10.02 (s, 1 H), 8.52 (s, 1 H), 7.86 (d, J = 9.8 Hz, 1 H), 7.74 (d, J = 9.8 Hz, 1 H), 3.50 (m, J = 6.7 Hz, 1 H), 1.60 (d, J = 6.7 Hz, 6 H). Anal. Calcd for $C_{10}H_{11}N_3O$: C, 63.48; H, 5.86; N, 22.21. Found: C, 63.33; H, 5.76; N, 22.18.

2-Isopropyl-[1,2,4]triazolo[1,5-*a*]pyridine-6-carbaldehyde (24). 2-Isopropyl-[1,2,4]triazolo[1,5-*a*]pyridine-6-carbaldehyde (**24**) was synthesized following the same reaction conditions as those for **23**, except that instead of being quenched with 10 wt % aqueous citric acid, 1 N HCl or water was used. Stirring the aqueous mixture for 2 h leads to complete rearrangement. The product was crystallized for X-ray determination by slow evaporation from ethyl acetate and hexanes; mp = 99.7−99.9 °C. R_f (silica gel; ethyl acetate) = 0.56. ^{1}H NMR (500 MHz, $CDCl_3$): δ 10.02 (s, 1 H), 9.02 (s, 1 H), 7.98 (d, J = 9.3 Hz, 1 H), 7.76 (d, J = 9.3 Hz, 1 H), 3.33 (m, J = 6.7 Hz, 1 H), 1.48 (d, J = 6.7 Hz, 6 H).

6-[4-(4-Fluoro-phenyl)-oxazol-5-yl]-3-isopropyl-[1,2,4]-triazolo[4,3-*a*]pyridine (25). To a stirred solution of 3-isopropyl-[1,2,4]triazolo[4,3-*a*]-6-pyridinecarboxaldehyde (0.30 g, 1.58 mmol) in 5 mL of acetonitrile was added α-(*p*-toluensulfonyl)-4-fluorobenzylisonitrile (0.55 g, 1.90 mmol) followed by powdered potassium carbonate (0.33 g, 2.37 mmol) at 22 °C. The mixture was stirred for 16 h at 22 °C and 24 h at 70 °C. The mixture was cooled to 22 °C, diluted with water, and extracted with chloroform (3×). The combined organic extracts were washed with water and brine, dried (sodium sulfate), and filtered. Concentration of the filtrate gave 0.59 g of a yellow solid, which was purified by flash chromatography, eluting with chloroform/methanol (97:3), to give 0.5 g (98%) of 6-[4-(4-fluoro-phenyl)-oxazol-5-yl]-3-isopropyl-[1,2,4]triazolo[4,3-*a*]-pyridine as a white solid: mp 213 °C. ^{1}H NMR (500 MHz, $CDCl_3$): δ 8.21 (s, 1 H), 8.04 (s, 1 H), 7.85 (d, J = 9.8 Hz, 1 H), 7.64 (m, 2 H), 7.42 (d, J = 9.8 Hz, 1 H), 7.16 (m, 2 H), 3.34 (m, 1 H), 1.53 (d, J = 7.3 Hz, 6 H). Anal. Calcd for $C_{18}H_{15}FN_4O$: C, 67.07; H, 4.69; N, 17.38; F, 5.89. Found: C, 67.07; H, 4.62; N, 17.48; F, 6.02.

Acknowledgment. The authors would like to thank Dr. Jon Bordner and Ivan Samardjiev for the small-molecule X-ray structure determinations on compounds **17**, **23**, and **24**. We also thank Chris Williams from Chemical Computing Group Inc. for his support. We are grateful to Drs. Frank M. DiCapua and Alan Mathiowetz for the review of the manuscript and helpful discussions.

Supporting Information Available: Details on construction of the p38 homology model and X-ray crystallographic data for compounds **17**, **23**, and **24**. This material is available free of charge via the Internet at http://pubs.acs.org.

References

(1) Langmuir, I. Isomorphism, Isosterism and Covalence. *J. Am. Chem. Soc.* **1919**, *41*, 1543−1559.
(2) Freidman, H. L. *Influence of Isosteric Replacement Upon Biological Activity*; National Academy of Sciences − National Research Council Publication No. 206; U.S. Government Printing Office: Washington DC, 1951, pp 295−357.
(3) Thornber, C. W. Isosterism and Molecular Modification in Drug Design. *Chem. Soc. Rev.* **1979**, *8*, 563−580.
(4) Badger, A. M.; Griswold, D. E.; Kapadia, R.; Blake, S.; Swift, B. A.; Hoffman, S. J.; Stroup, G. B.; Webb, E.; Rieman, D. J.; Gowen, M.; Boehm, J. C.; Adams, J. L.; Lee, J. C. Disease-modifying activity of SB 242235, a selective inhibitor of p38 mitogen-activated protein kinase, in rat adjuvant-induced arthritis. *Arthritis Rheum.* **2000**, *43*, 175−183.
(5) Jackson, J. R.; Bolognese, B.; Hillegass, L.; Kassis, S.; Adams, J.; Griswold, D. E.; Winkler, J. D. Pharmacological effects of SB 220025, a selective inhibitor of P38 mitogen-activated protein kinase, in angiogenesis and chronic inflammatory disease models. *J. Pharmacol. Exp. Ther.* **1998**, *284*, 687−692.
(6) Wadsworth, S. A.; Cavender, D. E.; Beers, S. A.; Lalan, P.; Schafer, P. H.; Malloy, E. A.; Wu, W.; Fahmy, B.; Olini, G. C.; Davis, J. E.; Pellegrino-Gensey, J. L.; Wachter, M. P.; Siekierka, J. J. RWJ 67657, a Potent, Orally Active Inhibitor of p38 Mitogen-Activated Protein Kinase. *J. Pharmacol. Exp. Ther.* **1999**, *291*, 680−687.
(7) Tong, L.; Pav, S.; White, D. M.; Rogers, S.; Crane, K. M.; Cywin, C. L.; Brown, M. L.; Pargellis, C. A highly specific inhibitor of human p38 MAP kinase binds in the ATP pocket. *Nat. Struct. Biol.* **1997**, *4*, 311−316.
(8) Wilson, K. P.; McCaffrey, P. G.; Hsiao, K.; Pazhanisamy, S.; Galullo, V.; Bemis, G. W.; Fitzgibbon, M. J.; Caron, P. R.; Murcko, M. A.; Su, M. S. The structural basis for the specificity of pyridinylimidazole inhibitors of p38 MAP kinase. *Chem. Biol.* **1997**, *4*, 423−431.
(9) Wang, Z.; Canagarajah, B. J.; Boehm, J. C.; Kassisa, S.; Cobb, M. H.; Young, P. R.; Abdel-Meguid, S.; Adams, J. L.; Goldsmith, E. J. Structural basis of inhibitor selectivity in MAP kinases. *Structure* **1998**, *6*, 1117−1128.
(10) Stelmach, J. E.; Liu, L.; Patel, S. B.; Pivnichny, J. V.; Scapin, G.; Singh, S.; Hop, C. E.; Wang, Z.; Strauss, J. R.; Cameron, P. M.; Nichols, E. A.; Keefe, S. J.; Neill, E. A.; Schmatz, D. M.; Schwartz, C. D.; Thompson, C. M.; Zaller, D. M.; Doherty, J. B. Design and synthesis of potent, orally bioavailable dihydroquinazolinone inhibitors of p38 MAP kinase. *Bioorg. Med. Chem. Lett.* **2003**, *13*, 277−280.
(11) Wang, Z.; Harkins, P. C.; Ulevitch, R. J.; Han, J.; Cobb, M. H.; Goldsmith, E. J. The structure of mitogen-activated protein kinase p38 at 2.1-Å resolution. *Proc. Natl. Acad. Sci. U.S.A.* **1997**, *94*, 2327−2332.
(12) Dombroski, M. A.; Letavic, M. A.; McClure, K. F.; Barberia, J. T.; Carty, T. J.; Cortina, S. R.; Csiki, C.; Dipesa, A. J.; Elliott, N. C.; Gabel, C. A.; Jordan, C. K.; Labasi, J. M.; Martin, W. H.; Peese, K. M.; Stock, I. A.; Svensson, L.; Sweeney, F. J.; Yu, C. H. Benzimidazolone p38 inhibitors. *Bioorg. Med. Chem. Lett.* **2004**, *14*, 919−923.
(13) de Dios, A.; Shih, C.; de Uralde, B. L.; Sánchez, C.; del Prado, M.; Cabrejas, L. M. M.; Pleite, S.; Blanco-Urgoiti, J.; María José Lorite; Nevill, C. R., Jr.; Bonjouklian, R.; York, J.; Vieth, M.; Wang, Y.; Magnus, N.; Campbell, R. M.; Anderson, B. D.; McCann, D. J.; Giera, D. D.; Lee, P. A.; Schultz, R. M.; Li, L. C.; Johnson, L. M.; Wolos, J. A. Design of Potent and Selective 2-Aminobenzimidazole Based p38α MAP Kinase Inhibitors with Excellent in Vivo Efficacy. *J. Med. Chem.* **2005**, *48*, 2270−2273.
(14) Nobeli, I.; Price, S. L.; Lommerse, J. P. M.; Taylor, R. Hydrogen bonding properties of oxygen and nitrogen acceptors in aromatic heterocycles. *J. Comput. Chem.* **1997**, *18*, 2060−2074.
(15) Mao, L.; Wang, Y.; Liu, Y.; Hu, X. Molecular Determinants for ATP-binding in Proteins: A Data Mining and Quantum Chemical Analysis. *J. Mol. Biol.* **2004**, *336*, 787−807.
(16) Davis, A. M.; Teague, S. J. Hydrogen Bonding, Hydrophobic Interactions, and Failure of the Rigid Receptor Hypothesis. *Angew. Chem., Int. Ed.* **1999**, *38*, 736−749.
(17) Murray, J. S.; Ranganathan, S.; Politzer, P. Correlations between the Solvent Hydrogen Bond Acceptor Parameter β and the Calculated Molecular Electrostatic Potential. *J. Org. Chem.* **1991**, *56*, 3734−3737.
(18) Kollman, P.; McKelvey, J.; Johansson, A.; Rothenberg, S. Theoretical Studies of Hydrogen-Bonded Dimers. Complexes Involving HF, H_2O, NH_3, HCl, H_2S, PH_3, NCN, HNC, HCP, CH_2NH, H_2CS, H_2CO, CH_4, CF_3H, C_2H_2, C_2H_4, C_6H_6, F^-, and H_3O^+. *J. Am. Chem. Soc.* **1975**, *97*, 955−965.
(19) Henry, J. R.; Rupert, K. C.; Dodd, J. H.; Turchi, I. J.; Wadsworth, S. A.; Cavender, D. E.; Schafer, P. H.; Siekierka, J. J. Potent inhibitors of the MAP kinase p38. *Bioorg. Med. Chem. Lett.* **1998**, *8*, 3335−3340.
(20) Henry, J. R.; Rupert, K. C.; Dodd, J. H.; Turchi, I. J.; Wadsworth, S. A.; Cavender, D. E.; Fahmy, B.; Olini, G. C.; Davis, J. E.; Pellegrino-Gensey, J. L.; Schafer, P. H.; Siekierka, J. J. 6-Amino-2-(4-fluorophenyl)-4-methoxy-3- (4-pyridyl)-1H-pyrrolo[2,3-b]-pyridine (RWJ 68354): A Potent and Selective p38 Kinase Inhibitor. *J. Med. Chem.* **1998**, *41*, 4196−4198.

(21) Abramov, Y. A.; Volkov, A.; Coppens, P. Anisotropic atom−atom potentials from X-ray charge densities: application to intermolecular interactions and lattice energies in some biological and nonlinear optical materials. *J. Mol. Struct. (THEOCHEM)* **2000**, *529*, 27−35.
(22) Stone, A. J. *The Theory of Intermolecular Forces*; Oxford University Press: Oxford, 1996.
(23) Jin, P.; Murray, J. S.; Politzer, P. Local ionization energy and local polarizability *Int. J. Quantum Chem.* **2004**, *96*, 394−401.
(24) Mancera, R. L.; Buckingham, A. D. Temperature Effects on the Hydrophobic Hydration of Ethane. *J. Phys. Chem.* **1995**, *99*, 14632−14640.
(25) Raschke, T. M.; Tsai, J.; Levitt, M. Quantification of the hydrophobic interaction by simulations of the aggregation of small hydrophobic solutes in water. *Proc. Natl. Acad. Sci. U.S.A.* **2001**, *98*, 5965−5969.
(26) Hansch, C.; Leo, A. *Exploring QSAR*; American Chemical Society: Washington, DC, 1995.
(27) Tsuzuki, S.; Honda, K.; Uchimaru, T.; Mikami, M.; Tanabe, K. Origin of Attraction and Directionality of the π/π Interaction: Model Chemistry Calculations of Benzene Dimer Interaction. *J. Am. Chem. Soc.* **2002**, *124*, 104−112.
(28) De Proft, F.; Geerlings, P. Conceptual and Computational DFT in the Study of Aromaticity. *Chem. Rev.* **2001**, *101*, 1451−1464.
(29) Revesz, L.; Di Padova, F. E.; Buhl, T.; Feifel, R.; Gram, H.; Hiestand, P.; Manning, U.; Zimmerlin, A. G. SAR of 4-hydroxypiperidine and hydroxyalkyl substituted heterocycles as novel p38 map kinase inhibitors. *Bioorg. Med. Chem. Lett.* **2000**, *10*, 1261−1264.
(30) Sisko, J.; Kassick, A. J.; Mellinger, M.; Filan, J. J.; Allen, A.; Olsen, M. A. An investigation of imidazole and oxazole syntheses using aryl-substituted TosMIC reagents. *J. Org. Chem.* **2000**, *65*, 1516−1524.
(31) Adams, J. L.; Gallagher, T. F.; Boehm, J. C.; Thompson, S. M. *6288062*; SmithKline Beecham Corporation: Philadelphia, 2001.
(32) Einhorn, J.; Einhorn, C.; Ratajczak, F.; Pierre, J.-L. Efficient and Highly Selective Oxidation of Primary Alcohols to Aldehydes by *N*-Chlorosuccinimide Mediated by Oxoammonium Salts. *J. Org. Chem.* **1996**, *61*, 7452−7454.
(33) Abarbri, M.; Dehmel, F.; Knochel, P. Bromine−magnesium-exchange as a general tool for the preparation of polyfunctional aryl and heteroarylmagnesium-reagents. *Tetrahedron Lett.* **1999**, *40*, 7449−7453.
(34) Potts, K. T.; Surapaneni, C. R. 1,2,4-Triazoles. XXV. The Effect of Pyridine Substitution on the Isomerization of s-Triazolo[4,3-a]pyridines into s-Triazolo[1,5-a]pyridines (1). *J. Heterocycl. Chem.* **1970**, *7*, 1019−1027.
(35) El Khadem, H. S.; Kawai, J.; Swartz, D. L. Synthesis and Rearrangements of Imidazolo- and Triazolo-Diazines. *Heterocycles* **1989**, *28*, 239−248.
(36) PDB accession code 1ZZL.
(37) Fitzgerald, C. E.; Patel, S. B.; Becker, J. W.; Cameron, P. M.; Zaller, D.; Pikounis, V. B.; O'Keefe, S. J.; Scapin, G. Structural basis for p38α MAP kinase quinazolinone and pyridol-pyrimidine inhibitor specificity. **2003**, *10*, 764−769.
(38) Deleted in proof.
(39) Andrews, P. R.; Craik, D. J.; Martin, J. L. Functional Group Contributions to Drug−Receptor Interactions. *J. Med. Chem.* **1984**, *27*, 1648−1657.
(40) Kunz, I. D.; Chen, K.; Sharp, K. A.; Kollman, P. A. The maximal affinity of ligands. *Proc. Natl. Acad. Sci. U.S.A.* **1999**, *96*, 9997−10002.
(41) Breneman, C. M.; Wiberg, K. B. Determining atom-centered monopoles from molecular electrostatic potentials. The need for high sampling density in formamide conformational analysis. *J. Comput. Chem.* **1990**, *11*, 361−373.
(42) Cossi, M.; Scalmani, G.; Rega, N.; Barone, V. New developments in the polarizable continuum model for quantum mechanical and classical calculations on molecules in solution. *J. Chem. Phys.* **2002**, *117*, 43−54.
(43) Cances, E.; Mennucci, B.; Tomasi, J. A new integral equation formalism for the polarizable continuum model: Theoretical background and applications to isotropic and anisotropic dielectrics. *J. Chem. Phys.* **1997**, *107*, 3032−3041.
(44) Frisch, M. J.; Trucks, G. W.; Schlegel, H. B.; Scuseria, G. E.; Robb, M. A.; Cheeseman, J. R.; Montgomery, Jr., J. A.; Vreven, T.; Kudin, K. N.; Burant, J. C.; Millam, J. M.; Iyengar, S. S.; Tomasi, J.; Barone, V.; Mennucci, B.; Cossi, M.; Scalmani, G.; Rega, N.; Petersson, G. A.; Nakatsuji, H.; Hada, M.; Ehara, M.; Toyota, K.; Fukuda, R.; Hasegawa, J.; Ishida, M.; Nakajima, T.; Honda, Y.; Kitao, O.; Nakai, H.; Klene, M.; Li, X.; Knox, J. E.; Hratchian, H. P.; Cross, J. B.; Bakken, V.; Adamo, C.; Jaramillo, J.; Gomperts, R.; Stratmann, R. E.; Yazyev, O.; Austin, A. J.; Cammi, R.; Pomelli, C.; Ochterski, J. W.; Ayala, P. Y.; Morokuma, K.; Voth, G. A.; Salvador, P.; Dannenberg, J. J.; Zakrzewski, V. G.; Dapprich, S.; Daniels, A. D.; Strain, M. C.; Farkas, O.; Malick, D. K.; Rabuck, A. D.; Raghavachari, K.; Foresman, J. B.; Ortiz, J. V.; Cui, Q.; Baboul, A. G.; Clifford, S.; Cioslowski, J.; Stefanov, B. B.; Liu, G.; Liashenko, A.; Piskorz, P.; Komaromi, I.; Martin, R. L.; Fox, D. J.; Keith, T.; Al-Laham, M. A.; Peng, C. Y.; Nanayakkara, A.; Challacombe, M.; Gill, P. M. W.; Johnson, B.; Chen, W.; Wong, M. W.; Gonzalez, C.; Pople, J. A. *Gaussian 03*, Revision B.04; Gaussian, Inc.: Wallingford, CT, 2004.
(45) *Spartan '02*, Wavefunction Inc: Irvine, CA.
(46) *ACD/Labs package*, release 6.0, Advanced Chemistry Development Inc: Toronto, Ontario, Canada.
(47) *MOE, Molecular Operating Environment*; Chemical Computing Group (Distributor): Montreal, Canada.

JM050346Q